Glutathione-responsive cyclodextrin-nanosponges as drug delivery systems for doxorubicin

Daga, Martina; de Graaf, Inge A. M.; Argenziano, Monica; Martinez Barranco, Ana Sofia ; Loeck, Maximillian; Al-Adwi, Yehya; Cucci, Marie Angele; Caldera, Fabrizio; Trotta, Francesco; Barrera, Giuseppina

Published in:
Toxicology in Vitro

DOI:
10.1016/j.tiv.2020.104800

Toxicology in Vitro 65 (2020) 104800

Contents lists available at ScienceDirect

Toxicology in Vitro

journal homepage: www.elsevier.com/locate/toxinvit

Glutathione-responsive cyclodextrin-nanosponges as drug delivery systems for doxorubicin: Evaluation of toxicity and transport mechanisms in the liver

Martina Daga[a], Inge A.M. de Graaf[b], Monica Argenziano[c], Ana Sofia Martinez Barranco[b], Maximillian Loeck[b], Yehya Al-Adwi[b], Marie Angele Cucci[a], Fabrizio Caldera[d], Francesco Trotta[d], Giuseppina Barrera[a], Angela Casini[e,***], Roberta Cavalli[c,**], Stefania Pizzimenti[a,*]

[a] Department of Clinical and Biological Sciences, University of Turin, Turin, Italy
[b] Groningen Research Institute of Pharmacy, University of Groningen, Groningen, the Netherlands
[c] Department of Drug Science and Technology, University of Turin, Turin, Italy
[d] Department of Chemistry, University of Turin, Turin, Italy
[e] Department of Chemistry, Technical University of Munich (TUM), Garching b. München, Germany

ARTICLE INFO

Keywords:
Glutathione-responsive nanosponges
β-Cyclodextrin
Doxorubicin
HepG2 cells
Rat precision-cut liver slices
Hepatotoxicity

ABSTRACT

The potential mammalian hepatotoxicity of a new class of GSH-responsive cyclodextrin-based nanosponges loaded with the anticancer drug doxorubicin (Dox-GSH-NS) was investigated. Previous studies showed that these nanosponges can release medicaments preferentially in cells having high GSH content, a common feature of chemoresistant cells, and showed enhanced anti-tumoral activity compared to free Dox *in vitro* and *in vivo* in cells with high GSH content. Following these promising results, we investigated here the Dox-GSH-NS hepatotoxicity in human HepG2 cells (*in vitro*) and in the organotypic cultures of rat precision-cut liver slices (PCLS, *ex vivo*), while their accumulation in rat liver was assessed *in vivo*. Moreover, the transport in Dox uptake, as well as its efflux, was studied *in vitro*. Overall, benefiting of the integration of different investigational models, a good safety profile of Dox-GSH-NSs was evidenced, and their hepatotoxicity resulted to be comparable with respect to free Dox both *in vitro* and *ex vivo*. Furthermore, *in vivo* studies showed that the hepatic accumulation of the Dox loaded in the NS is comparable with respect to the free drug. In addition, Dox-GSH-NSs are taken up by active mechanisms, and can escape the efflux drug pump, thus, contributing to overcoming drug resistance.

1. Introduction

Nanomedicine is a rapidly spreading area of medical research, due to important applications in diagnosis and treatments of human diseases, including cancer (Wang et al., 2011). Several types of nanoparticles (NPs) for tumor treatment are currently under investigation (Duchene et al., 2016; Marano et al., 2016; Caldera et al., 2018), and some of them, containing chemotherapeutic drugs such as doxorubicin (Dox), are already approved for clinical purposes (Anselmo and Mitragotri, 2016). Stimuli-responsive NPs represent a new opportunity in advanced drug delivery systems, allowing a sustained drug release in response to an external stimulus present in the microenvironment, such as light, temperature, pH, or redox gradient (Cheng et al., 2011, 2014). For example, glutathione (GSH)-responsive NPs enable the controlled drug release in response to the intracellular GSH concentration (Cheng et al., 2011), which is about 1000-fold higher intracellularly than in extracellular matrices (Traverso et al., 2013). Moreover, chemoresistant cancer cells show even higher levels of GSH (Traverso et al., 2013). Thus, GSH-sensitive nanosystems are attractive because they can release the drug preferentially within cells, compared to the extracellular environment, and feature an enhanced drug release in chemoresistant cells.

Recently, a new class of GSH-responsive cyclodextrin-based nanosponges (GSH-NS) have been characterized (Trotta et al., 2016; Daga et al., 2016). The synthesis was achieved in a single step in presence of β-cyclodextrin, 2-hydroxyethyl disulfide, and pyromellitic dianhydride as crosslinking agent (Fig. 1).

The presence of the disulfide bridges in the 2-hydroxyethyl disulfide molecules makes the structure susceptible to the cleavage by reducing agents, in particular by GSH. Dox was incorporated into the polymeric

* Correspondence to: S. Pizzimenti, Dep. of Clinical and Biological Sciences, University of Turin, Corso Raffaello 30, 10125 Turin, Italy.
** Correspondence to: R. Cavalli, Dep. of Drug Science and Technology, University of Turin, Via Pietro Giuria 9, 10125 Turin, Italy.
*** Correspondence to: A. Casini, Department of Chemistry, Technical University of Munich (TUM), Lichtenbergstr. 4, 85748 Garching b. München, Germany.
E-mail addresses: angela.casini@tum.de (A. Casini), roberta.cavalli@unito.it (R. Cavalli), stefania.pizzimenti@unito.it (S. Pizzimenti).

https://doi.org/10.1016/j.tiv.2020.104800
Received 21 November 2019; Received in revised form 27 January 2020; Accepted 15 February 2020
Available online 19 February 2020
0887-2333/

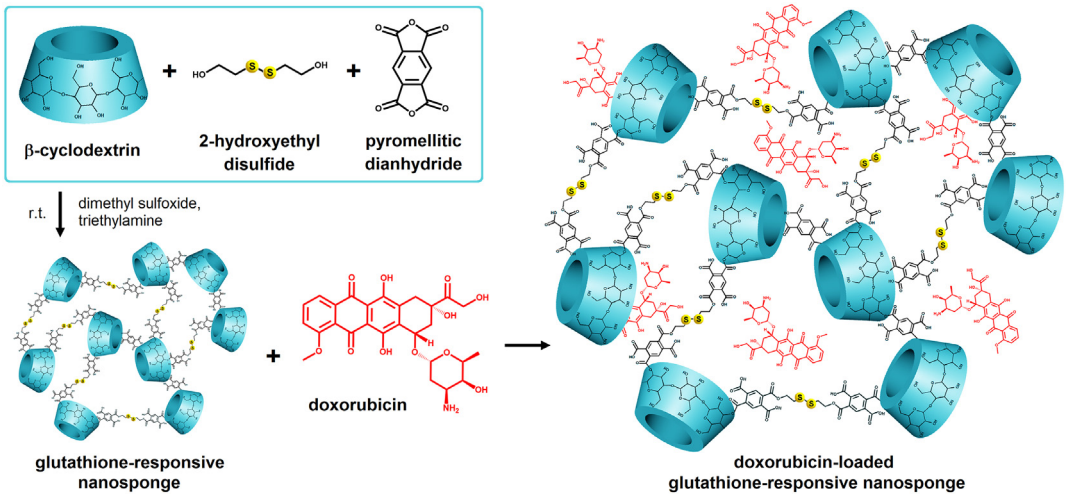

Fig. 1. Scheme of the doxorubicin-loaded glutathione-responsive nanosponge (Dox-GSH-NSs) synthesis. After the one-step synthesis of GSH-responsive nanosponges (GSH-NS), doxorubicin was incorporated into the polymeric matrix.

matrix by adding the drug to the aqueous GSH-NS nanosuspension, thus, obtaining doxorubicin-loaded GSH-NS (Dox-GSH-NS) (Trotta et al., 2016; Daga et al., 2016).

Interestingly, Dox (Daga et al., 2016) or strigolactone analogues (Argenziano et al., 2018) loaded into GSH-NS showed enhanced anticancer properties in different tumor cell lines featuring high GSH content. Most importantly, GSH-NS-Dox formulations reduced the development of human prostate cancer in xenograft models more than free Dox (Daga et al., 2016). Having established the effectiveness of the NPs formulation in tumor cells, toxicology studies represent the next crucial step in drug discovery. Previous results showed that the *in vivo* administration of Dox-GSH-NS, compared to that of Dox, did not elicit any enhancement in mice cardiotoxicity (Daga et al., 2016), which is the major adverse effect of Dox administration (Takemura and Fujiwara, 2007). Thus, in the present study our attention focused on hepatotoxicity for two main reasons: on the one hand it is well-known that Dox can cause liver toxicity (Bagchi et al., 1995); furthermore, it has been shown that this organ, being one of the main filters of the human body, can capture the exogenous nanoparticles in the circulation, leading to toxicity (Zhang et al., 2016). Reasons for liver accumulation of NPs may include the sheer size of the liver (Bartneck et al., 2014), its highly fenestrated endothelium (Abdel-Misih and Bloomston, 2010), as well as the high number of Kupffer cells, the resident macrophages in the liver (Baboci et al., 2020; Kretzschmar, 1996). Moreover, compared to other organs, the liver contains relatively high concentrations of GSH (Kretzschmar, 1996).

Among the liver cell models to study hepatotoxicity, the HepG2 human hepatocarcinoma cell line represents a widely used alternative to freshly isolated liver hepatocytes. The latter are considered the gold standard model for cytotoxicity studies (Guillouzo et al., 2007), but have complicated isolation procedures, high inter-individual variability, limited lifespan, and high cost, constituting serious limitations for their use in toxicological studies (Madan et al., 2003) Immortalized liver-derived cell lines can overcome these limitations, and HepG2 cells are particularly attractive because they are highly differentiated and display many of the genotypic features of normal liver cells (Rudzok et al., 2010).

However, two-dimensional (2D) cell cultures cannot always accurately predict toxicity *in vivo* because they are not representative of the three-dimensional (3D) complexity of tissues. In this context, the *ex vivo* rat precision-cut liver slice (PCLS) model has gained attention (de Graaf et al., 2007, 2010) since it preserves the structure and cell types of the liver, including Kupffer cells, proposed as the main cellular component responsible for nanoparticle accumulation in the liver (Olinga et al., 2001; Samuelsson et al., 2017), as well as cell-cell and cell-matrix extracellular interactions. Recently, several studies have used this technology to study the toxicity and the tissue accumulation mechanisms of different anticancer drugs and supramolecular drug delivery systems (Bertrand et al., 2014; Estrada-Ortiz et al., 2017; Spreckelmeyer et al., 2017; Han et al., 2018). Of note, the PCTS system is uniquely suited to examine molecular responses to toxicant exposures and compare species differences, and is nowadays a FDA-approved technology (Groothuis et al., 2014).

In this study, we present results on Dox-GSH-NS hepatotoxicity, uptake/efflux mechanisms and liver accumulation, using *in vitro*, *ex vivo,* and *in vivo* models. Specifically, we evaluated the effects of the NS on cell viability and Dox uptake both *in vitro* (HepG2 cells) and *ex vivo* (PCLS). Moreover, in both models, we studied the contribute of active transport mechanisms in Dox uptake, as well as its efflux, in particular focusing our attention on the transmembrane P-glycoprotein (P-gp), which can transport out of cells a large variety of cytotoxic substances, including Dox (Higgins, 2007). Finally, we evaluated liver accumulation of Dox in the NS formulation with respect to the free drug treatment in animals.

2. Materials and methods

2.1. Preparation and characterization of GSH-NS, Dox-GSH-NS, and 6-coumarin-GSH-NS

GSH-NS and Dox-GSH-NS were prepared as previously described (Daga et al., 2016; Argenziano et al., 2018). 6-Coumarin-GSH-NS were prepared by adding the fluorescent marker 6-coumarin (0.1 mg/ml) (Sigma-Aldrich, USA) to the aqueous nanosuspension of GSH-NS (10 mg/ml) and stirring for 24 h at room temperature (r.t.) in the dark. The physical-chemical profile of the GSH-NS formulations was characterized *in vitro*. Average diameter, polydispersity index and surface charge of GSH-NS, blank, 6-Coumarin and Dox loaded, were measured by dynamic light scattering using a 90 Plus particle sizer (Brookhaven Instruments Corporation, USA). For the analyses, a dilution of GSH-NS samples with distilled water at ratio 1:30 *v*/v was carried out. The DLS measurements were performed at a fixed angle of 90° and at a temperature of 25 °C. For Zeta potential determination, the diluted samples were placed in the electrophoretic cell, where an electric field of approximately 15 V/cm was applied. The quantitative determination of Dox in the Dox-GSH-NS formulation was performed using a reverse phase HPLC method, as previously described (Daga et al., 2016; Argenziano et al., 2018). A fluorescence detector, set at excitation and

emission wavelengths of 480 and 560 nm, respectively, was used for Dox detection.

The loading capacity and encapsulation efficiency of Dox-GSH-NS were determined on solid samples, obtained by freeze-drying. A Dox-GSH-NS freeze-dried sample was dispersed in 5 ml of water and sonicated for 15 min. After centrifugation (15,000 rpm, 10 min) the supernatant was analyzed by HPLC, to measure Dox concentration in the GSH-NS. The loading capacity and encapsulation efficiency were calculated, according to the following equations:

$$\text{Loading capacity (\%)} = [\text{amount of Dox/weight of Dox} - \text{GSH} - \text{NS}] \times 100$$

$$\text{Encapsulation efficiency (\%)} = [\text{amount of DOX loaded/total amount of DOX}] \times 100$$

2.2. Release profile of Dox from GSH-NS

In vitro drug release experiments were carried out by the dialysis bag technique, using a dialysis membrane of cellulose (Spectrapore, cut-off 12,000 Da). One ml of Dox-GSH-NS was placed in the donor chamber. The receiving compartment contained 1 ml of phosphate buffered saline (PBS) 1 × at pH 5.5 or 7.4, to investigate the influence of pH on the Dox release profile from GSH-NS. The receiving phase was withdrawn at regular intervals and completely replaced with the same amount of fresh solution, to maintain sink conditions. The concentration of Dox in the withdrawn samples was detected by HPLC (Daga et al., 2016).

2.3. HepG2 cell line and culture conditions

HepG2 cell line (American Type Culture Collection, USA) was maintained in a humidified atmosphere of 5% CO_2 at 37 °C in Dulbecco's modified Eagle's medium supplemented with 10% fetal bovine serum, 100 U/ml penicillin, 100 μg/ml streptomycin (Euroclone, Italy).

2.4. HepG2 viability assay

The toxic effect of Dox and Dox-GSH-NS was determined in HepG2 cells through the 3-(4,5-dimethyl thiazol-2-yl)-2,5-diphenyltetrazolium bromide (MTT) (Sigma-Aldrich) assay. This colorimetric assay, able to determine the level of metabolic activity in cells, may be interpreted as a measure of both cell viability and cell proliferation (Sylvester, 2011). Cells were seeded (1.500 cells/well) in 96-well plates with 200 μl of serum-supplemented medium, and were allowed to attach for 24 h. Afterwards, cells were treated with 0.5, 1, 5, 10, and 50 μM of Dox or Dox-GSH-NS. Moreover, cells were incubated with the empty vehicles (GSH-NS) at dilutions corresponding to that of Dox-GSH-NS. The MTT assay was performed as previously reported (Daga et al., 2016), at 24 h, 48 h and 72 h from the beginning of the treatment, respectively. The half maximal effective concentration (EC_{50}) was calculated at 72 h by using a AAT Bioquest EC_{50} calculator (AAT Bioquest, Inc., Sunnyvale, *CA*. https://www.aatbio.com/tools/ec50-calculator).

2.5. Cellular uptake of Dox and Dox-GSH-NS and quantitative determination of Dox internalization

The internalization of Dox and Dox-GSH-NS was measured at different time points after the drug addition by taking advantage of the red fluorescence of Dox. HepG2 were seeded onto culture plates and incubated with Dox or Dox-GSH-NS 10 μM at 37 °C, and collected at different time points. Dox red fluorescence was visualized with a fluorescence microscope (Axiovert 35, Zeiss), or quantified by cytofluorimetric analysis (flow cytometry, BD AccuriTM), or by HPLC in cell lysates (Daga et al., 2016).

2.6. Evaluation of GSH-NS internalization in HepG2 cells

The GSH-NS internalization was determined by using fluorescent 6-coumarin-GSH-NSs. HepG2 cells were cultured in 6-well plates for 24 h to achieve approximately 80% confluence. Internalization of 6-coumarin-GSH-NSs was analyzed by fluorescence microscopy (Axiovert 35, Zeiss).

2.7. Temperature inhibition of active transport in HepG2 cells

To determine if the uptake of nanosponges was through active or passive transport, we compared the uptake in HepG2 of Dox-GSH-NS at 37 °C with the uptake at 4 °C, where all active processes such as endocytosis are inhibited. The time course of Dox incorporation was performed by visualization of red fluorescence by using a fluorescence microscope, as above described. Moreover, the effect of temperature on GSH-NS internalization was also analyzed by comparing the uptake of 6-coumarin-GSH-NS at 37 °C and 4 °C in HepG2 cells.

2.8. P-gp inhibition study in HepG2 cells

To investigate the role of the P-gp transporter in Dox efflux, HepG2 cells were pre-incubated 1 h in the absence and presence of the inhibitor PSC833 (2 μM) (Sigma-Aldrich). After pre-incubation, Dox or Dox-GSH-NS (10 μM) were added to the cell cultures, and the analysis of Dox cellular uptake was performed by cytofluorimetry as described above.

2.9. Animals for rat precision-cut liver slice (PCLS) studies

Male Wistar rats (weight *ca.* 220–250 g, aged 7/8 weeks) were purchased from Harlan (Horst, the Netherlands). Rats were housed in a temperature- and humidity-controlled on a 12/12 h light/dark cycle with free access to food (Harlan diet 2918, Harlan) and tap water. Tap water quality is constantly monitored by the *Inspectie Leefomgeving en Transport* (ILT) in the Netherlands. Rats were climatized at least 7 days before use. All the animal experiments were approved by the animal ethical committee of the University of Groningen.2.10 Preparation and Incubation of rat PCLSRats were anesthetized with 5% isofluorane/O_2. The liver was excised and placed in ice-cold University of Wisconsin (UW) organ preservation solution (DuPont Critical Care, IL) until further use. The PCLS were prepared following the protocol described by de Graaf and collaborators (de Graaf et al., 2010) with minor changes. Cores with a diameter of 5 mm were drilled from fresh rat liver using a hollow cylinder drill. The cores were sliced using a Krumdieck tissue slicer (Alabama R&D, USA), as already described (de Graaf et al., 2010). The obtained PCLS had an average thickness of approximately 250 μm and a wet weight of 5 mg. The slices were pre-incubated for 1 h at 37 °C in 12-well plates containing medium, as previously reported (de Graaf et al., 2010). The incubators had a constant flow of carbogen and were shaking at a speed of 90× per minute. Pre-incubation served to revitalise the slices before the experiment since metabolism and vitality are impaired due to slicing (by mechanical stress and cold). After the pre-incubation, slices were brought onto new plates with fresh medium and were incubated at 37 °C, or 4 °C. Control slices were incubated without any treatment.

2.10. ATP content of PCLS

The viability of the PCLS was determined for indicated time points and for each treatment (control, plain Dox, Dox-GSH-NS) by determining the ATP content in each slice as described by de Graaf and collaborators (de Graaf et al., 2007) The ATP content was corrected by the protein amount of each slice, as already reported (Han et al., 2018).

2.11. Quantification of Dox uptake in PCLS

The overall Dox concentration in the slices was determined by measuring the fluorescence of the drug. The slices were harvested at the indicated incubation times in triplicate in individual vials and stored at −20 °C until the analysis. For the analysis, the slices were homogenised in 1 ml 1:1 ethanol (100%): 0.3 M HCl using a Mini-BeadBeater 24 (Biospec Products, Bartlesville, USA) and subsequently centrifuged at 15.600 *g* for 5 min at r.t. 100 µl of supernatant and a calibration curve (2–8 µM) diluted 1:1 in ethanol (100%): 0.3 M HCl were brought onto a black 96-well plate. The auto-mix function prior to readings was disabled except when indicated differently. Fluorescence was measured at λ_{ex} = 540 nm and λ_{em} = 590 nm using a Gemini XPS Microplate Reader (Molecular Devices, USA). Dox concentrations are expressed as nmol/slice.

2.12. Temperature inhibition of active transport in PCLS

To determine if the uptake of nanosponges was through active or passive transport, and to study the time-course of this uptake, PCLS were pre-incubated for 1 h as previously described. After pre-incubation, slices were transferred into fresh pre-cooled or pre-warmed medium Williams medium E (WME) (de Graaf et al., 2010) at 4 °C or 37 °C (80% O_2 and 5% CO_2) and incubated for 0, 15, 30, 60 and 120 min with a 10 µM Dox-GSH-NS or Dox solution. For this assay, Dox was used as a control since it is known to enter cells also through a passive diffusion process. After incubation, all slices were washed in 500 µl blank PBS 1× in order to remove any free drug and nanosponge residues. Afterward, slices were introduced into Eppendorf cups and snap-frozen in liquid nitrogen. Samples were stored at −20 °C until further analysis.

2.13. P-gp inhibition study in PCLS

PCLS were pre-incubated for 1 h with and without PSC833 (2 µM). Afterward, 10 µM Dox or 10 µM GSH-NS-Dox were added into each well, followed by 2 h of incubation. After incubation, slices were rinsed in 500 µl of blank cold PBS 1× and frozen in liquid nitrogen. Samples were stored at −20 °C.

2.14. Preparation of cryosections for confocal laser microscopy to analyze Dox fluorescence and Kupffer cell fluorescent immunostaining

To better visualize the Dox distribution within the slices by confocal microscopy, we have slightly modified the protocol by prolonging the pre-incubation PCLS time (3 h instead of 1 h), since this diminished unspecific signal from Dox binding to dead cells on the slices edges. PCLS were embedded in KP-cryocompound (Klinipath, NL) and frozen in methylbutane (Sigma-Aldrich) on dry ice. Afterward, slices were stored in −80 °C freezer until cutting. Sections of 4 µm were cut by using a Cryostar NX70 cryostat (Thermofisher Scientific, Germany) and placed on adhesive microscope glass slides (Klinipath). Sections were fixed using formalin 4% and mounted using Mowiol mounting medium before being examined under Leica SP8 confocal laser microscopy (Leica, Germany). Two different wavelengths or sequences were applied to localize Dox after treatments: Alexa 488 to visualize PCLS tissue (green), and Alexa 546 to visualize Dox inside PCLS (red).

For the fluorescent immunostaining of Kupffer cells, 4 µm cryosections were dried at r.t. for at least 20 min. Subsequently, the sections were fixated and permeabilised in acetone at r.t. for 5 min. Thereafter, the macrophage marker CD163 primary antibody (ED2, 1:500) was applied for 60 min in the dark at r.t.. Then, after washing the sections in PBS, an Alexa 555 labelled (Life Technologies, US) secondary antibody was added (1:100) for 30 min in the dark at r.t.. Unspecific binding of the secondary antibody was inhibited by using 5% normal rat serum. Finally, the sections were counterstained with DAPI for 3 min and immediately embedded - after washing in Mowiol mounting medium then covered with a glass coverslip. Three different wavelengths were applied: Alexa 488 to visualize PCLS tissue (green), DAPI to visualize cell nuclei (blue), and Alexa 555 to visualize Kupffer cells (red).

2.15. In vivo studies of drug accumulation in the liver

Male Wistar rats (weight *ca.* 250–270 g, aged 8/10 weeks) were maintained on a standard normocaloric rat diet (4RF21 certificate PF1610, Mucedola S.r.l., Settimo Milanese, Milan, Italy), and tap water *ad libitum*. Tap water quality is constantly monitored by the *Società Metropolitana Acque Torino* (SMAT) Italy. All the animal experiments were approved by the animal ethical committee of the University of Turin. Dox or Dox-GSH-NS in PBS 1×, were administered by tail injection into the lateral caudal vein, at the dose of 1 mg/kg. 24 rats were divided randomly into two groups (3 rats per each time point; 4 time points for each treatment). At the desired times after treatments, rats were anesthetized with isoflurane/O_2 (induction 5%, maintenance 3%), and livers were collected, washed with cold saline solution, dried over filter papers, weighed and frozen at −80 °C until analysis. Tissue extracts were prepared as already described (Daga et al., 2016). Dox content was performed by HPLC analysis, as previously reported (Fundarò et al., 2000).

2.16. Statistical analysis

Data were expressed as means ± SD. Significance between experimental groups was determined by one-way ANOVA followed by the Bonferroni multiple comparison post-test using GraphPad InStat software (San Diego, CA, USA). Values of $p \leq .05$ were considered statistically significant.

3. Results

3.1. Characterization of GSH-NS, Dox-GSH-NS and 6-coumarin-GSH-NS

The GSH-responsive cyclodextrin-based nanosponges (GSH-NS) were synthesized according to previously established protocol (Trotta et al., 2016; Daga et al., 2016). Dox or 6-coumarin were incorporated into the polymeric matrix, by adding them to the aqueous GSH-NS nanosuspension, as already reported (Trotta et al., 2016; Daga et al., 2016). Sizes, polydispersity indices, and Zeta potentials of GSH-NS, Dox-GSH-NS, and 6-coumarin-GSH-NS were evaluated by *dynamic light scattering,* and values are reported in Table 1. According to our previous reports (Trotta et al., 2016; Daga et al., 2016), the average diameters ranged about 200–210 nm, with a smaller size for the blank ones. The Zeta potentials were also determined and are comparable for the various formulations, with values of *ca.* −30 mV, indicating a larger electrostatic repulsion between particles which ensures the physical stability and avoid aggregation of the nanoformulations. The polydispersity index, a parameter of the nanoparticle size distribution, showed values around 0.20, indicating a moderately disperse distribution. GSH-NS were able to efficiently load Dox, showing an encapsulation efficiency of 94% and loading capacity of 12%, in line with previously reported data (Trotta et al., 2016; Daga et al., 2016).

Table 1
Physico-chemical characteristics of free and loaded GSH-NS formulations.

Formulation	Diameter (nm)[a]	Polydispersity index[a]	Zeta potential (mV)[a]
GSH-NS	202.5 ± 14.2	0.20 ± 0.01	−32.4 ± 2.6
Dox-GSH-NS	210.6 ± 16.5	0.22 ± 0.02	−28.5 ± 3.2
6-coumarin-GSH-NS	208.8 ± 18.3	0.20 ± 0.01	−26.9 ± 2.8

[a] Values represent mean ± SD (n = 4).

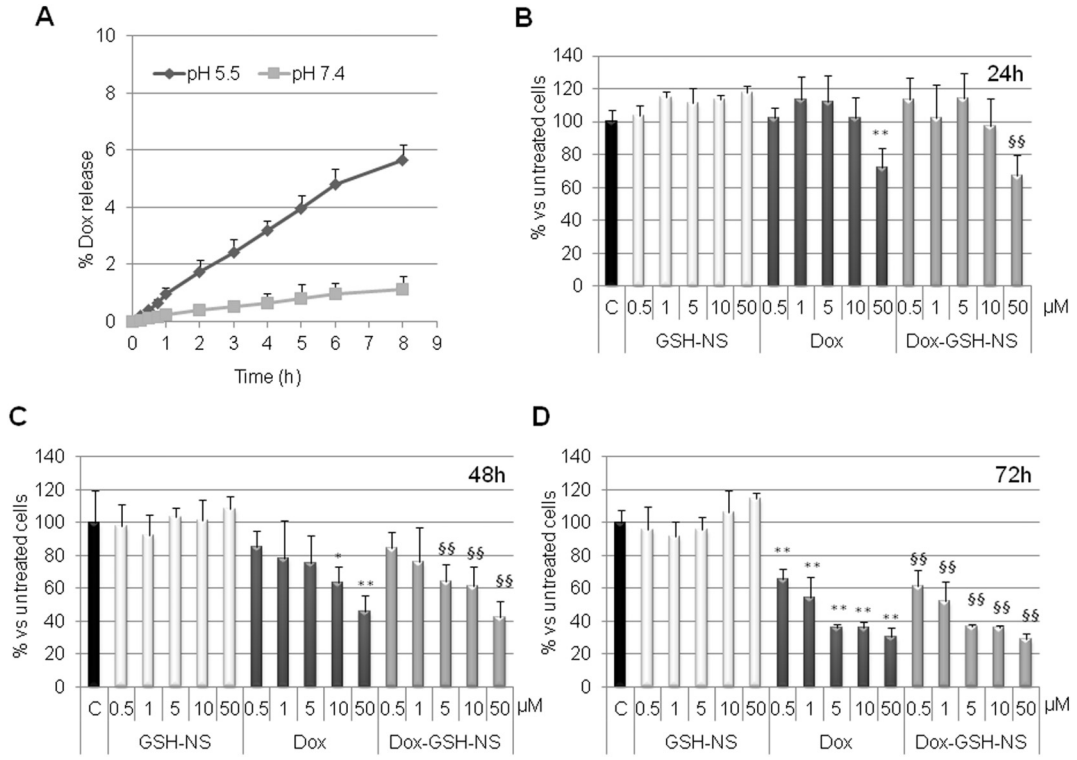

Fig. 2. (A) Release kinetics of Dox from GSH-NS at different pH (5.5 and 7.4). (B, C, D) GSH-NS, Dox and Dox-GSH-NS toxicity evaluated by MTT assay in HepG2 cells at the indicated concentration and incubation time. Results are expressed as percent of control values, as the mean ± SD ($N = 3$). * $p \leq .05$ and ** $p \leq .01$ *vs.* controls (c); § p ≤ .05 and §§ p ≤ .01 *vs* GSH-NS.

Table 2
Antiproliferative effects (EC_{50}) of Dox and Dox-GSH-NS against HepG2 cells at 72 h.

Drug	EC_{50} (µM)[a]
Dox	1.1 ± 0.57
Dox-GSH-NS	0.93 ± 0.58

[a] Values represent mean ± SD ($n = 3$).

3.2. Drug release studies

The *in vitro* release kinetic of Dox from GSH-NS was assessed by the dialysis bag technique. Dox-GSH-NS samples were placed in the donor chamber, while the receiving compartment contained phosphate buffered saline (PBS) 1× at pH 5.5 or 7.4, to investigate the influence of pH on the Dox release profile from GSH-NS (Fig. 2A). The drug release profile was consistently slow and prolonged over time and no initial burst effect was observed. At pH 7.4 the rate of drug release was lower than that measured at pH 5.5. The cumulative percent release of Dox from the GSH-NS was approximately 1% at pH 7.4 compared to 5.66% at pH 5.5 after 8 h, indicating that release was enhanced at acidic pH.

3.3. In vitro - effects of Dox and Dox-GSH-NS on HepG2 cell viability

The toxicity of both Dox and Dox-GSH-NS treatments was initially evaluated in HepG2 cells *in vitro*, using the classical MTT test at different incubation times (see experimental for details). As shown in Fig. 2B-D, a progressive dose-dependent inhibition of cell growth was observed which reached the maximum at 72 h incubation. However, there was no difference in toxicity between Dox and Dox-GSH-NS at any concentration or time tested. Moreover, the cells were treated with the empty vehicles (GSH-NS) at dilutions corresponding to that of Dox-GSH-NS, and any toxic effect was observed at any of the tested concentrations.

It should be noted that previously reported studies on the same nanoformulations showed a marked increase of Dox antitumoral activity in human colon and prostate cancer cells with high GSH content with respect to free Dox (Daga et al., 2016). Here, HepG2 cells are used as a model for drug hepatotoxycity studies by virtue of their high similarity to the normal liver cells (Rudzok et al., 2010), having very efficient detoxification systems, so that Dox could be metabolized very quickly, with the effect of lowering its toxicity. In fact, the antiproliferative effects of the Dox-GSH-NS were studied in HepG2 cells over timein comparison to free Dox. Table 2 reports the calculated EC_{50} values after 72 h incubation, when the cytotoxic effect reaches its maximum, and the results show that both treatments have similar EC_{50} values, around 1 µM. As expected, the toxicity of the drug-loaded NS is not increased in this cellular model.

3.4. In vitro - Dox uptake in HepG2 cells

After incubation of HepG2 cells with Dox or Dox-GSH-NS (10 µM) at 37 °C, free Dox was internalized more slowly than the drug carried by GSH-NS, as shown by the analysis of the red fluorescence intensity of Dox by cytofluorimetry. Indeed, the red fluorescence signal (Fig. 3A) was around two-fold more intense in Dox-GSH-NS treated cells with respect to plain Dox, at all times analyzed, starting from 15 up to 120 min. Similar results were obtained by measuring the Dox content by High Performance Liquid Chromatography (HPLC) (Fig. 3B), and by visualization of red fluorescence of Dox with a fluorescence microscope (Fig. 4A).

In order to investigate whether the uptake of the GSH-NS takes place by active or passive transport, HepG2 cells were also incubated at 4 °C in parallel with the incubation at 37 °C. The results obtained by the cytofluorimetric analysis showed that at 4 °C the uptake of Dox-GSH-NS was significantly lower compared to the uptake of Dox-GSH-NS at 37 °C at all the time tested (Fig. 3A). Similar results were also obtained by HPLC analysis (Fig. 3B) and by fluorescence microscopy (Fig. 4).

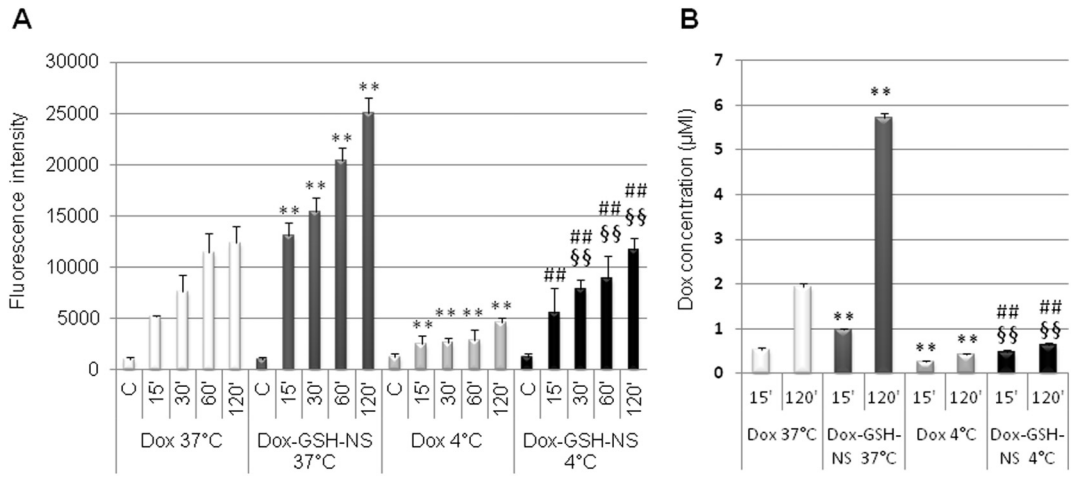

Fig. 3. Analysis of red fluorescence intensity of Dox by cytofluorimeter (A) and HPLC (B) in HepG2 cells treated with Dox or Dox-GSH-NS 10 μM at 37 °C and 4 °C, respectively, and collected at the indicated times (min). The results are the mean ± SD ($N = 3$). $^{**}p \leq .01$ *vs* Dox 37 °C at the corresponding time (CT); §§ $p \leq .01$ *vs* Dox 4 °C at the CT; ## $p \leq .01$ *vs* Dox-GSH-NS 37 °C at the CT. (For interpretation of the references to colour in this figure legend, the reader is referred to the web version of this article.)

Overall, these results support the idea that active transport mechanisms are in place for the Dox-GSH-NS drug conjugates.

Moreover, in agreement with other reports (Dalmark and Storm, 1981; Majumdar et al., 2009) the uptake of free Dox at 4 °C was lower with respect to its uptake at 37 °C (Figs. 3 and 4). Since this drug was reported to enter cells by a passive diffusion mechanism (Speelmans et al., 1994), it has been proposed that the reduction of temperature leads to an increase of Dox aggregation, which in turn can affect its entry into cells (Dalmark and Storm, 1981). However, recently an active transport of Dox has also been described (Lee et al., 2017). Thus, both ATP-dependent and independent mechanisms can be responsible for the overall Dox uptake.

To further detect the internalization of GSH-NSs into the cells, we performed fluorescence microscopy analysis on labelled 6-coumarin-GSH-NS. We selected 6-coumarin as a fluorescent marker because it can strongly interact with the nanosponge matrix, forming a stable system. Moreover, being insoluble in water, its release from nanosponges is negligible over time. Therefore, it is possible to evaluate if fluorescent NS *per se* are easily taken up by the cells, as previously reported (Daga et al., 2016; Gigliotti et al., 2016). At 37 °C, the fluorescent nanoparticles were internalized within 15 min into HepG2 cells and their accumulation significantly increased at 120 min incubation (Fig. 5). Instead, the incubation at 4 °C inhibited the 6-coumarin-GSH-NS internalization, thus, further corroborating the idea that active transport mechanisms play a role in the uptake of NS.

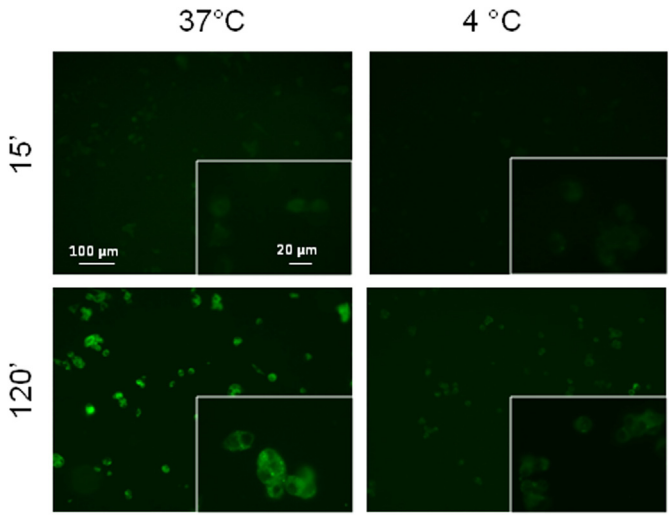

Fig. 5. Fluorescent images of 6-coumarin-GSH-NSs uptake in HepG2 cells at the indicated time (min) and temperature. Green fluorescence of 6-coumarin was examined by using fluorescence microscopy (454 nm). (For interpretation of the references to colour in this figure legend, the reader is referred to the web version of this article.)

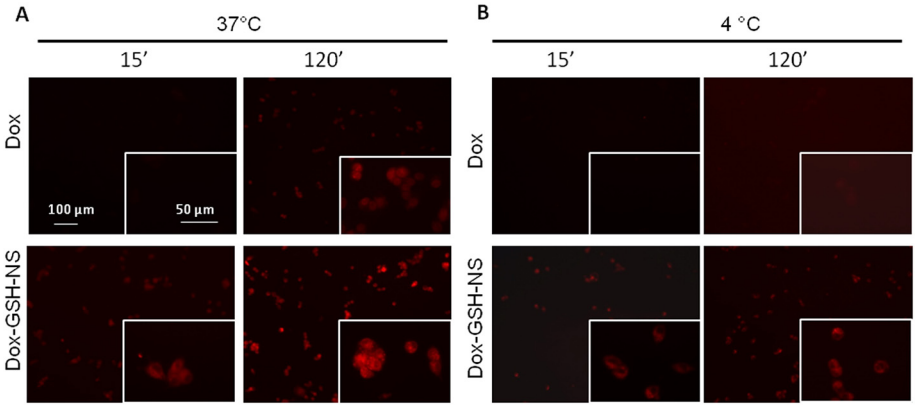

Fig. 4. Internalization of Dox and Dox-GSH-NS 10 μM in HepG2 at the indicated time (min) at 37 °C and (A) at 4 °C (B). Red fluorescence of Dox was examined by using fluorescence microscopy (580 nm). (For interpretation of the references to colour in this figure legend, the reader is referred to the web version of this article.)

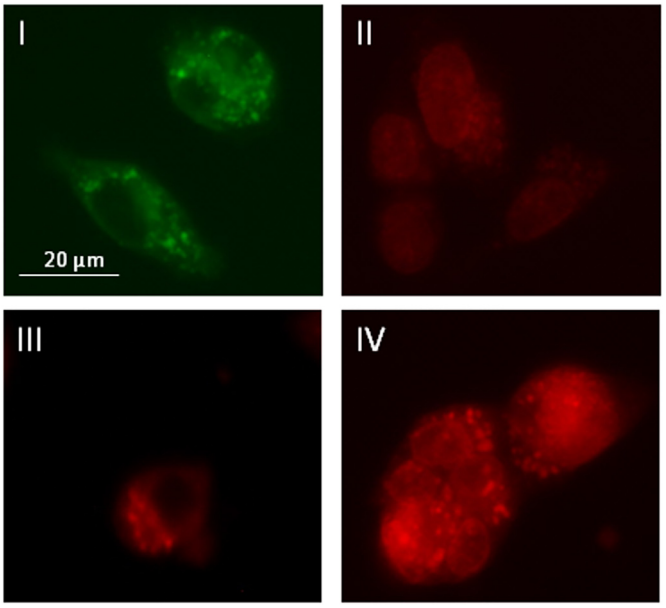

Fig. 6. Fluorescent sub-cellular localization in HepG2 cells of 6-coumarin-GSH-NS at 120 min, 37 °C (I), 10 µM Dox at 120 min, 37 °C (II), 10 µM Dox-GSH-NS at 15 min (III), and 120 min (IV), 37 °C.For interpretation of the references to colour in this figure legend, the reader is referred to the web version of this article.)

3.5. In vitro - sub-cellular localization of GSH-NS, Dox, and Dox-GSH-NS in HepG2 cells

In order to evaluate the sub-cellular localization of the nanosponges, HepG2 cells were incubated at different times with 0.3 µM 6-coumarin-GSH-NSs, 10 µM Dox, and 10 µM Dox-GSH-NS at 37 °C, as reported in the experimental section. Fluorescent images of each treatment are shown in Fig. 6. It is possible to observe that in HepG2 cells treated with 6-coumarin-GSH-NSs the fluorescence is contained in intracellular vesicles (I). A similar pathway is observed in the cytosol of the Dox-GSH-NS treated cells at early time (15 min) (III), as well as at 120 min (IV). At this time, it is possible to observe also a diffuse and marked nuclear localization, which is not so pronounced in the case of free Dox at 120 min (II).

3.6. In vitro - P-gp inhibition in HepG2 cells

Beside the studies on drug influx, our research continued by delving into the mechanisms of drug efflux. In particular, we focused our attention on the transmembrane glycoprotein P-gp, which can acts as an efflux pump for a large variety of cytotoxic substances, including Dox, thereby decreasing their cytotoxicity (Higgins, 2007). The over-expression of P-gp is one of the well-known mechanisms of multidrug resistance, which is the most important cause of failure for chemotherapy (Kapse-Mistry et al., 2014). Thus, we investigated the role of the P-gp transporter in the accumulation efficiency of free Dox and Dox-GSH-NS at 37 °C. P-gp was inhibited by pre-incubating, HepG2 cells for 1 h with 2 µM of P-pg inhibitor PSC833 (Atadja et al., 1998). Then, Dox or Dox-GSH-NS (10 µM) were added and cells were collected at the indicated time. The red fluorescence intensity of Dox was analyzed by cytofluorimetry (Fig. 7). A significant accumulation of Dox was observed after 120 min in HepG2 cells co-treated with PSC833, when compared with cells treated only with Dox. No differences were observed in cells treated with Dox-GSH-NS, pre-incubated or not with the inhibitor, indicating that the P-gp transporter may not play a role in the efflux mechanisms of the nanosponges.

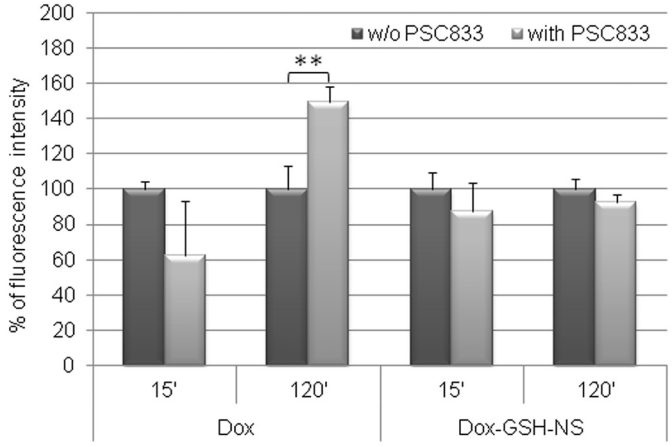

Fig. 7. Analysis of red fluorescence intensity of Dox by cytofluorimeter in HepG2 cells treated with Dox or Dox-GSH-NS (10 µM) at 37 °C, pre-treated with PSC833 or not (w/o PSC833) at the indicated time (min). The fluorescence values of pre-treated PSC833 samples were calculated as the percentage of the values obtained in the corresponding PSC833-non-treated samples. The results are expressed as mean ± SD ($N = 3$). $^{**}p \leq .01$. For interpretation of the references to colour in this figure legend, the reader is referred to the web version of this article.)(For interpretation of the references to colour in this figure legend, the reader is referred to the web version of this article.)

3.7. Ex vivo - effects of GSH-NS, Dox and Dox-GSH-NS on rat PCLS viability

Afterwards, the toxicity of the Dox-GSH-NS system was studied *ex vivo* in rat PCLS. The slices viability was assessed measuring the ATP content after 24 h treatment with different concentrations of Dox and Dox-GSH-NS (0–100 µM). The results are presented in Fig. 8A. Starting from 10 µM, dose-dependent liver toxicity in rat PCLS treated with Dox or Dox-GSH-NS was observed with respect to the untreated rat PCLS. Dox induced *ca.* 50% reduction of PCLS viability at *ca.* 10 µM concentration. Comparing the viability of PCLS treated with Dox-GSH-NS with that of slices incubated with the same concentration of free Dox, no statistically significant difference could be recorded at any tested concentration. Moreover, the rat PCLS were treated with the empty vehicles (GSH-NS) at dilutions corresponding to those of Dox-GSH-NS (see experimental for details), and no toxicity could be observed at any tested concentration (Fig. 8A). Overall, the data further support the benefit of the drug formulation in the selected nanosponges.

3.8. Ex vivo - analysis of Dox uptake and transport mechanism in rat PCLS

The analysis of Dox incorporation after the treatment of rat PCLS with 10 µM free Dox and Dox-GSH-NS at 37 °C was performed by measurement of the fluorescence of Dox in the slice homogenates (see experimental for details). As shown in Fig. 8B, Dox accumulates equally in the PCLS over time, as either free drug or in the nanosponge formulation.

To establish the difference between active transport and passive diffusion of plain Dox and Dox-GSH-NS, PCLS were treated with both formulations and incubated at either 37 °C or 4 °C. Thus, Dox uptake was evaluated after 30, 120 and 240 min by HPLC. While at 37 °C no substantial difference can be observed between the various treatments, Dox-GSH-NS at 4 °C accumulated significantly less after 30 and 120 min compared to free Dox at 4 °C. Moreover, Dox-GSH-NS at 4 °C accumulated significantly less after 30, 120 and 240 min compared to Dox-GSH-NS at 37 °C (Fig. 9A), further corroborating the idea of an active transport mechanism for NS uptake.

Afterward, the role of P-gp transporter in the uptake efficiency of plain Dox and Dox-GSH-NS at 37 °C was investigated in rat PCLS. Thus, PCLS were pre-incubated for 1 h in the absence and presence of the

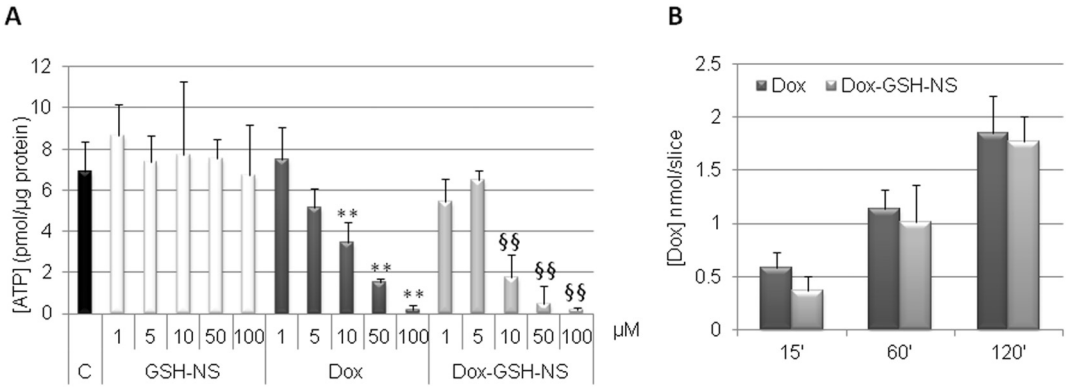

Fig. 8. (A) Rat PCLS viability, measured in [ATP] (pmol/µg protein) at 24 h, after incubation at 37 °C with plain Dox, Dox-GSH-NS at the indicated concentrations, or without treatment (c). Results are expressed as mean ± SD of three independent experiments, each performed on three livers. $^{**}p \leq .01$ *vs* c; §§ $p \leq .01$ *vs* GSH-NS. (B) Analysis of Dox uptake in rat PCLS incubated at 37 °C with 10 µM plain Dox or Dox-GSH-NS, by HPLC at the indicated time (min) and measured as [Dox] nmol/slice. Data are expressed as mean ± SD ($N = 6$).

specific P-gp inhibitor PSC833 (2 µM); then, either Dox or GSH-NS-Dox were added into each well, followed by 15 min and 120 min incubation. As shown in Fig. 9B, any significant difference between PSC833-treated and non-treated groups could be found. Furthermore, it is interesting to note that also free Dox accumulation did not show any difference after incubation with the P-gp inhibitor, at variance with the HepG2 cell studies.

The uptake of Dox and Dox-GSH-NS was further studied in PCLS by confocal fluorescence microscopy. As mentioned in the experimental section, we decided to slightly modify the incubation protocol (from 1 h to 3 h pre-incubation) with the aim to enhance the quality of the images under confocal microscopy of Dox- and Dox-GSH-NS-treated PCLS. After 3 h pre-incubation, PCLS were treated for 3 h with Dox or Dox-GSH-NS. The corresponding confocal images are shown in Fig. 10. A higher accumulation of Dox inside PCLS was observed after Dox-GSH-NS treatment (Fig. 10B) comparing to free Dox incubation (Fig. 10A). This result is in line with the observations made in the case of the HepG2 cells. Untreated PCLS showed no fluorescent signal (Fig. 10C).

Fluorescent immunostaining of Kupffer cells (ED2) was also performed in PCLS (Fig. 10D) and the fluorescent pattern obtained was different between Dox- or Dox-GSH-NS-treated PCLS (Fig. 10A and B). Although it was not possible to show the ED2 staining and Dox fluorescence on the same sections, these results suggest that Dox is not taken up specifically by Kupffer cells.

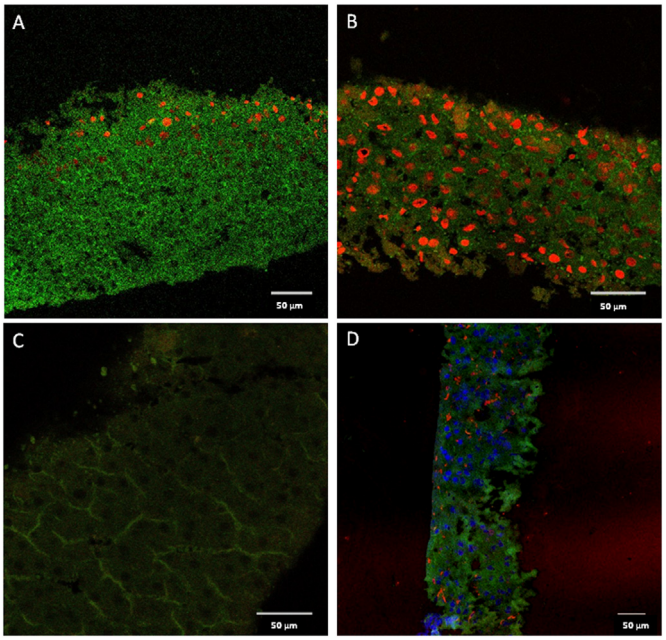

Fig. 10. Confocal microscopy images of PCLS cryosections after 3 h of incubation with 10 µM Dox (A) or 10 µM Dox-GSH-NS (B) or untreated (C). PCLS tissue autofluorescence: green; Dox: red. (D) Confocal microscopy image of PCLS cryosection stained with Kupffer cell marker ED2 (red), and DAPI (blue). PCLS tissue autofluorescence: green; DAPI-stained nuclei: blue; Kupffer cells: red. (For interpretation of the references to colour in this figure legend, the reader is referred to the web version of this article.)

3.9. In vivo - Dox accumulation in liver

The accumulation of Dox and Dox-GSH-NS in rat liver was determined at 0.5, 6 and 24 h after i.v. administration (Table 3). Dox accumulated very quickly in the liver, starting from 30 min. The levels

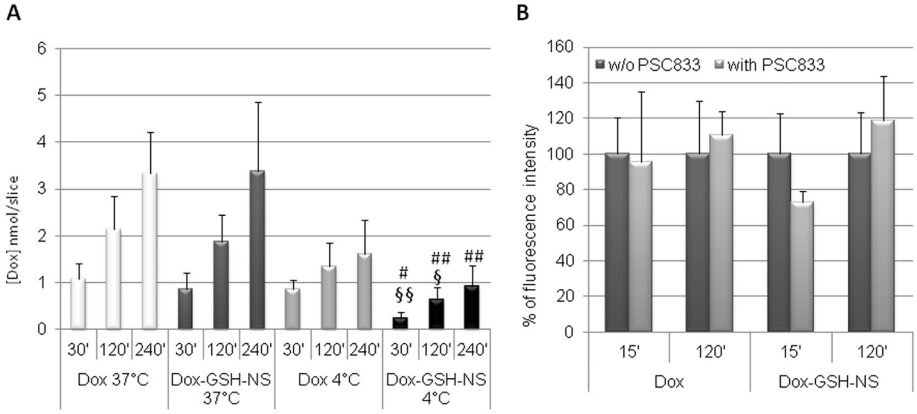

Fig. 9. (A) The uptake of Dox into PCLS after Dox or Dox-GSH-NS 10 µM treatments at 37 °C or 4 °C incubation. The uptake was measured at the indicated time (min) and is given as [Dox] nmol/slice. Results are expressed as mean ± SD of four independent experiments, each performed on three livers. § $p \leq .05$ and §§ $p \leq .01$ *vs* Dox 4 °C at the corresponding time (CT); # $p \leq .05$ ## $p \leq .01$ *vs* Dox-GSH-NS 37 °C at the CT. (B) Dox uptake into PCLS after Dox or Dox-GSH-NS (10 µM) treatments at 37 °C, with the P-pg inhibitor PSC833 or not (w/o PSC833) at the indicated time (min). The [Dox] values of pre-treated PSC833 samples were calculated as the percentage of the values obtained in the corresponding PSC833-not treated samples. The results are expressed as mean ± SD ($N = 3$).

Table 3
Accumulation of Dox and Dox-GSH-NS in rat liver.

Time (hours)	Dox (μg Dox/g tissue)[a]	Doxo-GSH-NS (μg Dox/g tissue)[a]
0.5	7.73 ± 0.09	7.41 ± 0.38
6	7.72 ± 0.91	6.99 ± 0.29
24	5.38 ± 0.75[b]	5.49 ± 0.04[b]

[a] Values represent mean ± SD ($n = 3$).
[b] $p < .01$ *vs* respective 0.5 h.

are stable until 6 h, while at 24 h its concentration is significantly lower. No differences in Dox levels were observed between free Dox and Dox-GSH-NS-treated rats at any time tested.

4. Discussion and conclusions

The herewith reported Dox-GSH-NSs offer very promising application in cancer treatment. In fact, they are not only GSH-sensitive, which makes them particularly suitable for the treatment of chemoresistant cells (Daga et al., 2016), but also pH-sensitive, further enhancing the targeted treatment of cancer, in virtue of the more acidic environment of tumors, compared to the normal surrounding tissues (Karimi et al., 2016). Results on HepG2 cells, taken as a model for liver cells, demonstrated similar inhibition of cell viability of Dox-GSH-NSs with respect to free Dox, suggesting a safety use of the nanoformulation in the clinic. However, uptake studies showed a higher Dox level in Dox-GSH-NS-treated cells, probably due to a rapid and efficient intracellular accumulation of NS, as also demonstrated by the early fluorescence (15 min) observed in 6-coumarin-GSH-NS-treated HepG2. Higher Dox concentration observed at early time would elicit higher toxicity; nevertheless, as mentioned above, this was not observed. A possible explanation can arise from the very effective cellular detoxification systems in HepG2 cells, so that Dox could be metabolized very quickly, with the effect of lowering its toxicity. Further studies should be devoted to the characterization of the anticancer effects of Dox-GSH-NSs in suitable *in vivo* models of cancer.

Most nanoparticles are captured by the cells through endocytosis, a process that requires energy (Petros and DeSimone, 2010; Zeng et al., 2012, 2014). Our studies on cellular uptake under low-temperature condition are in agreement with these reports, suggesting that the uptake of Dox-GSH-NS in HepG2 cells is active. Fluorescence microscopy studies further confirm this mechanism, since the Dox-GSH-NS formulations accumulate in intracellular vesicles, presumably endosomes, consistent with cell entry through one of the varieties of possible endocytic pathways.

Concerning efflux mechanisms, the use of P-gp inhibitors, such as the cyclosporin analogue PSC833 can block the drug efflux, thus, enhancing drug toxicity. In our experimental conditions, PSC833 was able to affect the content of Dox, but not of Dox-GSH-NS-treated cells. These results are in agreement with several reports (Wielinga et al., 2000; Arora et al., 2011) and suggest that free Dox, which can be normally rapidly extruded by the pump, after treatment with PSC833 accumulates intracellularly. Conversely, the NS protects Dox from this efflux mechanism, which is bypassed, favoring drug's intracellular distribution and entry into the cell nucleus.

Our study continued with the evaluation of the toxicity of the drug-loaded nanosponges *ex vivo* in PCLS, considered a more predictive model than 2D cell cultures, and already used to test the hepatotoxicity of NPs (Dragoni et al., 2012). In this more physiologically relevant model, free Dox and Dox-GSH-NSs showed the same hepatotoxicity, as previously demonstrated in HepG2 cells. However, in contrast to what observed *in vitro*, the initial uptake study using HPLC analysis revealed that the drug equally accumulates in the PCLS pre-incubated for 1 h and treated with Dox and Dox-GSH-NS for additional 4 h (Fig. 9A). Most likely, this is due to the fact that the NS diffusion within the PCLS could be hampered by the interaction with the macromolecules of the extracellular matrix, completely absent in the 2D model (Barua and Mitragotri, 2014).

To better visualize the location of Dox in the liver slices by confocal microscopy, the PCLS were pre-incubated 3 h instead of 1 h, prior treatment exposure. Then, slices were treated with the two formulations, and after 3 h a higher Dox fluorescent signal was observed in the Dox-GSH-NS-treated PCLS compared to the free Dox-treated (Fig. 10), whereas HPLC quantitative results on Dox uptake up to 4 h showed similar values (Fig. 9A). Several reasons can explain this discrepancy, and very likely the different pre-incubation time may be the leading cause. Indeed, it is possible that the presence of debris surrounding the slice post-slicing, still present after 1 h of pre-incubation but not after 3 h, can interfere with the nanoformulation uptake. Confocal microscopy studies on Kupffer cells in PCLS further underline the safety of Dox-GSH-NS, since any selective drug accumulation could be observed in these cells, in contrast to what has been proposed by several authors, who demonstrated that Kupffer cells are the main cellular component responsible for drug-loaded nanoparticle accumulation in the liver (Samuelsson et al., 2017).

As previously shown in HepG2 cell, the temperature strongly affects Dox-GSH-NS uptake in PLCS. Thus, these results further strengthen the hypothesis of active transport of our NSs. However, in contrast to the *in vitro* studies, no effect of P-gp inhibition was observed in the liver slices. However, it should be noticed, that in slices the bile canaliculi (to where P-gp substrates are effluxed) tend to retain their contents (unpublished data), which makes it difficult to distinguish between Dox inside the cells and effluxed Dox, when measuring the content of a slice homogenate. In any case, the use of PCLS offers good opportunities to evaluate toxicity, uptake and accumulation of drugs in different organs and species, eventually leading to new insight into the effects in human tissues derived from patients. However, optimization of the experimental set-up to reduce the damage of the PCLS induced by culturing is still necessary to exclude possible interference on the obtained results.

Finally, the here presented *in vivo* studies showed that the Dox-loaded NSs accumulate in rat liver as the free Dox. In conclusion, Dox-GSH-NSs show a good safety profile, since they do not accumulate in the liver more than the free drug, have comparable toxicity with respect to the free drug, and can escape the efflux drug P-gp pump, thus, contributing to overcoming drug resistance when reaching the target cancerous cells. Moreover, the empty vector GSH-NS never caused cytotoxicity both *in vitro* and *ex vivo*, and can also be considered as a carrier for other chemotherapic drugs, further extending the possibilities towards its therapeutic applications.

Declaration of Competing Interest

The authors declare that they have no known competing financial interests or personal relationships that could have appeared to influence the work reported in this paper.

Acknowledgements

This work was supported by the University of Turin (Turin, Italy), assigned to SP, RC, MA, GB and by FONDAZIONE CRT (Turin, Italy), awarded to FT (grant number TROF_CRT_16_02).

References

Abdel-Misih, S.R., Bloomston, M., 2010. Liver anatomy. Surg. Clin. North Am. 90 (4), 643–653.
Anselmo, A.C., Mitragotri, S., 2016. Nanoparticles in the clinic. Bioeng Transl Med. 1 (1), 10–29.
Argenziano, M., Lombardi, C., Ferrara, B., Trotta, F., Caldera, F., Blangetti, M., Koltai, H., Kapulnik, Y., Yarden, R., Gigliotti, L., Dianzani, U., Dianzani, C., Prandi, C., Cavalli, R., 2018. Glutathione/pH-responsive nanosponges enhance strigolactone delivery to prostate cancer cells. Oncotarget. 9 (88), 35813–35829.

Arora, H.C., Jensen, M.P., Yuan, Y., Wu, A., Vogt, S., Paunesku, T., Woloschak, G.E., 2011. Nanocarriers enhance doxorubicin uptake in drug- resistant ovarian cancer cells. Cancer Res. 72 (3), 769–778.
Atadja, P., Watanabe, T., Xu, H., Cohen, D., 1998. PSC-833, a frontier in modulation of P-glycoprotein mediated multidrug resistance. Cancer Metastasis Rev. 17 (2), 163–168.
Baboci, L., Capolla, S., Di Cintio, F., Colombo, F., Mauro, P., Dal Bo, M., Argenziano, M., Cavalli, R., Toffoli, G., Macor, P., 2020. The dual role of the liver in nanomedicine as an actor in the elimination of nanostructures or a therapeutic target. J. Oncol, 2020:4638192.
Bagchi, D., Bagchi, M., Hassoun, E.A., Kelly, J., Stohs, S.J., 1995. Adriamycin-induced hepatic and myocardial lipid-peroxidation and DNA-damage, and enhanced excretion of urinary lipid metabolites in rats. Toxicology. 95 (1–3), 1–9.
Bartneck, M., Warzecha, K.T., Tacke, F., 2014. Therapeutic targeting of liver inflammation and fibrosis by nanomedicine. Hepatobiliary Surg Nutr. 3 (6), 364–376.
Barua, S., Mitragotri, S., 2014. Challenges associated with penetration of nanoparticles across cell and tissue barriers: a review of current status and future prospects. NanoToday. 9 (2), 223–243.
Bertrand, B., Stefan, L., Pirrotta, M., Monchaud, D., Bodio, E., Richard, P., Le Gendre, P., Warmerdam, E., de Jager, M.H., Groothuis, G.M., Picquet, M., Casini, A., 2014. Caffeine-based gold(I) N-heterocyclic carbenes as possible anticancer agents: synthesis and biological properties. Inorg. Chem. 53 (4), 2296–2303.
Caldera, F., Argenziano, M., Trotta, F., Dianzani, S., Gigliotti, L., Tannous, M., Pastero, L., Aquilano, D., Nishimoto, T., Higashiyama, T., Cavalli, R., 2018. Cyclic nigerosyl-1,6-nigerose-based nanosponges: an innovative pH and time-controlled nanocarrier for improving cancer treatment. Carbohydr. Polym. 194, 111–121.
Cheng, R., Feng, F., Meng, F., Deng, C., Feijen, J., Zhong, Z., 2011. Glutathione-responsive nano-vehicles as a promising platform for targeted intracellular drug and gene delivery. J. Control. Release 152 (1), 2–12.
Cheng, W., Gu, L., Ren, W., Liu, Y., 2014. Stimuli-responsive polymers for anti-cancer drug delivery. Mater. Sci. Eng. C Mater. Biol. Appl. 45, 600–608.
Daga, M., Ullio, C., Argenziano, M., Dianzani, C., Cavalli, R., Trotta, F., Ferretti, C., Zara, G.P., Gigliotti, C.L., Ciamporcero, E.S., Pettazzoni, P., Corti, D., Pizzimenti, S., Barrera, G., 2016. GSH-targeted nanosponges increase doxorubicin-induced toxicity "in vitro" and "in vivo" in cancer cells with high antioxidant defenses. Free Radic Biol Med. 97, 24–37.
Dalmark, M., Storm, H.H., 1981. Fickian diffusion transport process with features of transport catalysis. Doxorubicin transport in human red blood cells. J Gen Physiol. 78 (4), 349–364.
de Graaf, I.A., Groothuis, G.M., Olinga, P., 2007. Precision-cut tissue slices as a tool to predict metabolism of novel drugs. Expert Opin. Drug Metab. Toxicol. 3 (6), 879–898.
de Graaf, I.A., Olinga, P., de Jager, M.H., Merema, M.T., de Kanter, R., van de Kerkhof, E.G., Groothuis, G.M., 2010. Preparation and incubation of precision-cut liver and intestinal slices for application in drug metabolism and toxicity studies. Nat. Protoc. 5 (9), 1540–1551.
Dragoni, S., Franco, G., Regoli, M., Bracciali, M., Morandi, V., Sgaragli, G., Bertelli, E., Valoti, M., 2012. Gold nanoparticles uptake and cytotoxicity assessed on rat liver precision-cut slices. Toxicol. Sci. 128 (1), 186–197.
Duchene, D., Cavalli, R., Gref, R., 2016. Cyclodextrin-based polymeric nanoparticles as efficient carriers for anticancer drugs. Curr. Pharm. Biotechnol. 17 (3), 248–255.
Estrada-Ortiz, N., Guarra, F., de Graaf, I.A.M., Marchetti, L., de Jager, M.H., Groothuis, G.M.M., Gabbiani, C., Casini, A., 2017. Anticancer gold N-heterocyclic carbene complexes: a comparative in vitro and ex vivo study. Chem Med Chem. 12 (17), 1429–1435.
Fundarò, A., Cavalli, R., Bargoni, A., Vighetto, D., Zara, G.P., Gasco, M.R., 2000. (2000) Non- stealth and stealth solid lipid nanoparticles (SLN) carrying doxorubicin: pharmacokinetics and tissue distribution after i.v. administration to rats. Pharmacol. Res. 42 (4), 337–343.
Gigliotti, L., Minelli, R., Cavalli, R., Occhipinti, S., Barrera, G., Pizzimenti, S., Cappellano, G., Boggio, E., Conti, L., Fantozzi, R., Giovarelli, M., Trotta, F., Dianzani, U., Dianzani, C., 2016. In vitro and in vivo therapeutic evaluation of camptothecin-encapsulated β-cyclodextrin nanosponges in prostate cancer. J. Biomed. Nanotechnol. 12 (1), 114–127.
Groothuis, G.M.M., Casini, A., Meurs, H., Olinga, P., 2014. Translational research in pharmacology and toxicology using precision-cut tissue slices. In: Coleman (Ed.), Human-based Systems for Translational Research. 3. Royal Society Chemistry, Cambridge, UK, pp. 38–65.
Guillouzo, A., Corlu, A., Aninat, C., Glaise, D., Morel, F., Guguen-Guilluozo, C., 2007. The human hepatoma HepaRG cells: a highly differentiated model for studies of liver metabolism and toxicity of xenobiotics. Chem. Biol. Interact. 168 (1), 66–73.
Han, J., Räder, A.F.B., Reichart, F., Aikman, B., Wenzel, M.N., Woods, B., Weinmüller, M., Ludwig, B.S., Stürup, S., Groothuis, G.M.M., Permentier, H.P., Bischoff, R., Kessler, H., Horvatovich, P., Casini, A., 2018. Bioconjugation of supramolecular metallacages to integrin ligands for targeted delivery of cisplatin. Bioconjug. Chem. 29 (11), 3856–3865.
Higgins, C.F., 2007. Multiple molecular mechanisms for multidrug resistance transporters. Nature. 446 (7137), 749–757.
Kapse-Mistry, S., Govander, T., Srivastava, R., Yergeri, M., 2014. Nanodrug delivery in reversing multidrug resistance in cancer cells. Front. Pharmacol. 5, 159.
Karimi, M., Eslami, M., Sahandi-Zangabad, P., Mirab, F., Farajisafiloo, N., Shafaei, Z., Ghosh, D., Bozorgomid, M., Dashkhaneh, F., Hamblin, M.R., 2016. pH-sensitive stimulus-responsive nanocarriers for targeted delivery of therapeutic agents. Wiley Interdiscip. Rev Nanomed Nanobiotechnol. 8 (696–16).
Kretzschmar, M., 1996. Regulation of hepatic glutathione metabolism and its role in hepatotoxicity. Exp. Toxicol. Pathol. 48 (5), 439–446.
Lee, H.H., Leake, B.F., Kim, R.B., Ho, R.H., 2017. Contribution of organic anion-transporting polypeptides 1A/1B to doxorubicin uptake and clearance. Mol. Pharmacol. 91 (1), 14–24.
Madan, A., Graham, R.A., Carroll, K.M., Mudra, D.R., Burton, L.A., Krueger, L.A., Downey, A.D., Czerwinski, M., Forster, J., Ribadeneira, M.D., Gan, L.S., Lecluyse, E.L., Zech, K., Robertson Jr., P., Koch, P., Antonian, L., Wagner, G., Yu, L., Parkinso, A., 2003. Effects of prototypical microsomal enzyme inducers on cytochrome P450 expression in cultured human hepatocytes. Drug Metab. Dispos. 31 (4), 421–431.
Majumdar, S., Tejo, B.A., Badawi, A.H., Moore, D., Krise, J.P., Siahaan, T.J., 2009. Effect of modification of the physicochemical properties of ICAM-1-derived peptides on internalization and intracellular distribution in the human leukemic cell line HL-60. Mol. Pharm. 6 (2), 396–406.
Marano, F., Argenziano, M., Frairia, R., Adamini, A., Bosco, O., Rinella, L., Fortunati, N., Cavalli, R., Catalano, M.G., 2016. Doxorubicin-loaded nanobubbles combined with extracorporeal shock waves: basis for a new drug delivery tool in anaplastic thyroid cancer. Thyroid. 26 (5), 705–716.
Olinga, P., Merema, M.T., de Jager, M.H., Derks, F., Melgert, B.N., Moshage, H., Slooff, M.J., Meijer, D.K., Poelstra, K., Groothuis, G.M., 2001. Rat liver slices as a tool to study LPS-induced inflammatory response in the liver. J. Hepatol. 35 (2), 187–194.
Petros, R.A., DeSimone, J.M., 2010. Strategies in the design of nanoparticles for therapeutic applications. Nat. Rev. Drug Discov. 9 (8), 615–627.
Rudzok, S., Schlink, U., Herbarth, O., Bauer, M., 2010. Measuring and modeling of binary mixture effects of pharmaceuticals and nickel on cell viability/cytotoxicity in the human hepatoma derived cell line HepG2. Toxicol. Appl. Pharmacol. 244 (3), 336–343.
Samuelsson, E., Shen, H., Blanco, E., Ferrari, M., Wolfram, J., 2017. Contribution of Kupffer cells to liposome accumulation in the liver. Colloids Surf B Biointerfaces. 158, 356–362.
Speelmans, G., Staffhorst, R.W., de Kruijff, B., de Wolf, F.A., 1994. Transport studies of doxorubicin in model membranes indicate a difference in passive diffusion across and binding at the outer and inner leaflets of the plasma membrane. Biochemistry. 33 (46), 13761–13768.
Spreckelmeyer, S., Estrada-Ortiz, N., Prins, G.G.H., van der Zee, M., Gammelgaard, B., Stürup, S., de Graaf, I.A.M., Groothuis, G.M.M., Casini, A., 2017. On the toxicity and transport mechanisms of cisplatin in kidney tissues in comparison to a gold-based cytotoxic agent. Metallomics. 9 (12), 1786–1795.
Sylvester, P.W., 2011. Optimization of the tetrazolium dye (MTT) colorimetric assay for cellular growth and viability. Methods Mol. Biol. 716, 157–168.
Takemura, G., Fujiwara, H., 2007. Doxorubicin-induced cardiomyopathy from the cardiotoxic mechanisms to management. Prog. Cardiovasc. Dis. 49 (5), 330–352.
Traverso, N., Ricciarelli, R., Nitti, M., Marengo, B., Furfaro, A.L., Pronzato, M.A., Marinari, U.M., Domenicotti, C., 2013. Role of glutathione in cancer progression and chemoresistance. Oxidative Med. Cell. Longev. 2013, 972913.
Trotta, F., Caldera, F., Dianzani, C., Argenziano, M., Barrera, G., Cavalli, R., 2016. New glutathione bio-responsive cyclodextrin nanosponges. Chem Plus Chem. 81, 439–443.
Wang, A.Z., Langer, R., Farokhzad, O.C., 2011. Nanoparticle delivery of cancer drugs. Annu. Rev. Med. 63, 185–198.
Wielinga, P.R., Westerhoff, H.V., Lankelma, J., 2000. The relative importance of passive and P-glycopreotein mediated anthracycline efflux from multidrug –resistance cells. Eur. J. Biochem. 267 (3), 649–657.
Zeng, X., Zhang, Y., Nyström, A.M., 2012. Endocytic uptake and intracellular trafficking of bis-MPA-based hyperbranched copolymer micelles in breast cancer cells. Biomacromolecules. 1 (11), 3814–3822.
Zeng, X., Morgenstern, R., Nyström, A.M., 2014. Nanoparticle-directed sub-cellular localization of doxorubicin and the sensitization breast cancer cells by circumventing GST-mediated drug resistance. Biomaterials. 35 (4), 1227–1239.
Zhang, Y.N., Poon, W., Tavares, A.J., McGilvray, I.D., Chan, W.C.W., 2016. Nanoparticle-liver interactions: cellular uptake and hepatobiliary elimination. J. Control. Release 240, 332–348.